Polymer 267 (2023) 125647

Contents lists available at ScienceDirect

Polymer

journal homepage: www.elsevier.com/locate/polymer

Polymer materials derived from the SEAr reaction for gas separation applications

Laura Matesanz-Niño [a,b], Noelia Esteban [c], Matthew T. Webb [d], Aránzazu Martínez-Gómez [e], Fabián Suárez-García [f], Alfonso González-Ortega [b], Jesús A. Miguel [c], Laura Palacio [a], Michele Galizia [d,**], Cristina Álvarez [a,e], Ángel E. Lozano [a,c,e,*]

[a] SMAP, UA-UVA_CSIC, Research Unit Associated to CSIC, Faculty of Science, University of Valladolid, Paseo Belén 11, E-47011, Valladolid, Spain
[b] Department of Organic Chemistry, Faculty of Science, University of Valladolid, Paseo Belén 7, E-47011, Valladolid, Spain
[c] IU CINQUIMA, University of Valladolid, Paseo Belén 5, E-47011, Valladolid, Spain
[d] School of Chemical, Biological and Materials Engineering, University of Oklahoma, 100E. Boyd Street, Norman, OK, 73019, USA
[e] Institute of Polymer Science and Technology, ICTP-CSIC, Juan de la Cierva 3, E-28006, Madrid, Spain
[f] National Institute of Carbon, INCAR-CSIC, Dr. Ingeniero Francisco Pintado 26, E-33011, Oviedo, Spain

ARTICLE INFO

Keywords:
SEAr polycondensation reaction
Linear aromatic polymers
Porous polymer networks
Mixed matrix membranes
High thermal and chemical resistance materials
Gas separation

ABSTRACT

A set of linear polymers were synthesized utilizing an electrophilic aromatic substitution reaction (SEAr) between biphenyl and ketone containing electron-withdrawing groups (isatin, IS; N-methylisatin, MeIS; and 4,5-diazafluoren-9-one, DF). Optimization of the polycondensation reaction was made to obtain high molecular weight products when using DF, which has not previously been used for linear polymer synthesis. Due to the absence of chemically labile units, these polymers exhibited excellent chemical and thermal stability. Linear SEAr polymers were blended with porous polymer networks derived from IS and MeIS, and both neat/mixed materials were tested as membranes for gas separation. The gas separation properties of both pristine polymers and mixed matrix membranes were good, showing some polymer membrane CO_2 permeability values higher than 200 barrer.

1. Introduction

One of the most fascinating topics in polymer chemistry is the discovery of new polymer-forming reactions. Despite the wide variety of available synthetic methodologies in organic chemistry, not all pathways can be used to make useful polymers. Almost a century ago, it was observed that it is necessary to use very efficient (high yield) reactions to obtain high molecular weight polymers [1–4].

Despite intense research in this field during the last few decades, the search for new polymer-forming reactions continues to attract work, such as the acid-catalyzed condensation of ketones and aldehydes, having electron-withdrawing groups, with aromatic compounds, known as hydroxyalkylation [5–7]. Olah suggested the concept of superelectrophilic activation to explain the reactivities of some electrophiles in superacidic solutions [8–10]. This activation has been proposed in Friedel–Crafts-type reactions of 1,2-dicarbonyl groups, aldehydes, nitriles, ketones, and other systems [11,12]. However, the reactivity of non-activated ketones species, even in the presence of a low pKa acid, i.e., triflic acid (TFSA), does not proceed with high yields.

In the context of polycondensation processes, superacid-catalyzed polyhydroxylakylation reactions of carbonyl compounds, having electron-withdrawing groups substituents, with aromatic hydrocarbons have been able to produce high-molecular weight polymers. In these reactions, the intermediate alcohol moiety reacts with another aromatic compound to give a diarylation product. Thus, Zolotukhin obtained high molecular weight polymers by reaction of activated ketones, such as [2,2,2-trifluoroacetophenone (TFAP), 1H-indole-2,3-dione (isatin, IS), etc.], with several aromatic compounds (biphenyl, *p*-terphenyl, *p*-quaterphenyl, binaphtol, etc.), using superacids [6,13–15]. Because the reaction produces aromatic sp^2-sp^2 bonds, the thermal and chemical stability of these polymers, when the monomers have been well chosen, can be very high.

Abbreviations: SEAr, Electrophilic Aromatic Substitution Reaction.

* Corresponding author. Institute of Polymer Science and Technology, ICTP-CSIC, Juan de la Cierva 3, E-28006, Madrid, Spain.
** Corresponding author.
E-mail addresses: mgalizia@ou.edu (M. Galizia), lozano@ictp.csic.es (Á.E. Lozano).

https://doi.org/10.1016/j.polymer.2022.125647
Received 13 October 2022; Received in revised form 21 December 2022; Accepted 26 December 2022
Available online 29 December 2022

Recently, our group has developed new porous organic polymer networks (POPs) based on this synthetic methodology [16]. These crosslinked materials, derived from IS, TFAP and 4,5-diazafluoren-9-one (DF), exhibited high microporosity, excellent thermal and chemical stability, and high CO_2 adsorption capacity. Consequently, these POPs were studied for several applications: metal-catalysis [17], organo-catalysis [18] and also as fillers in mixed matrix membranes (MMMs) for gas separation [19–24].

The search for higher performing materials in gas separation is essential nowadays to mitigate the effects of global warming on human health. More efficient membrane materials are sought for greenhouse gases capture (mainly CO_2) while improving energy efficiencies of current industrial separations [25,26]. Additionally, polymer materials that perform well in aggressive environments and high temperatures are particularly demanded by the industry [27,28]. In this work, six linear aromatic polymers and copolymers were made by reacting biphenyl (BP) with three ketones, namely isatin (IS), N-methylisatin (MeIS) and 4,5-diazafluoren-9-one (DF). These polymers showed high molecular weight and adequate mechanical properties to be employed as gas separation membranes.

MMMs were prepared from these linear polymers by including 20% w/w loadings of POPs derived from 1,3,5-triphenylbenzene (135TPB) or triptycene (TRP) and IS or MeIS.

Gas transport properties of linear polymers and MMMs were measured to assess their potential application in gas separation.

2. Experimental

2.1. Materials

Biphenyl (BP) (99.5%), 1H-indole-2,3-dione (isatin, IS) (97%) and 1,3,5-triphenylbenzene (135TPB) (97%) were supplied from Sigma-Aldrich and triptycene (TRP) (97%) was supplied from ABCR. All of them were used without further purification. 4,5-diazafluoren-9-one (DF) was obtained using a procedure previously reported [17,29]. Details of the synthesis of 4,5-diazafluoren-9-one (DF) and N-methylisatin (MeIS) are provided in the supplementary information section (Section 1, SI).

Anhydrous chloroform ($CHCl_3$) and trifluoromethanesulfonic acid (triflic acid, TFSA) were obtained from Merck and Fluorochem, respectively, with a purity higher than 99%.

2.2. Synthesis of polymers and copolymers

A series of linear polymers and copolymers were prepared by a superacid catalyzed polyhydroxylakylation reaction of carbonyl compounds with aromatic hydrocarbons [11,13,30–33]. The reaction yield for all the polymers and copolymers was above 95%. They were manufactured using a stoichiometric ratio of electrophilic (ketone) to nucleophilic (benzidine) monomers (1/1 for monomers and 1/1/2 for copolymers).

As an example, the synthesis of the BP-DF-MeIS copolymer is described as follows:

A mixture of dried monomers (8.2 mmol of BP, 4.1 mmol of DF and 4.1 mmol of MeIS) and 6 mL of anhydrous $CHCl_3$ were added to a 50 mL three-neck flask, mechanically stirred under a static nitrogen atmosphere. After the monomers became fully dissolved, the reaction flask was immersed in an ice-water-salt bath at −5 °C and then TFSA (12.4 mL) was dropwise added by an addition funnel for 20 min. Subsequently, the reaction was maintained at 5 °C for 11 days. In the case of the polymers not having the DF monomer, the ice-water-salt bath was maintained for 30 min after the addition of TFSA and then the reaction was maintained at room temperature for 10 h.

Finally, the reaction products were poured into a methanol-water (2:1) mixture and stirred overnight. The precipitated polymer was washed in basic water (pH around 10), methanol-water (2:1), hot water, and finally in methanol. The product was collected by filtration and dried at 150 °C in a vacuum oven overnight.

2.3. Synthesis of porous polymer neworks, POPs

The porous polymer networks shown in Fig. 3 were obtained through methodology previously described by us [16,17]. Reaction yields for all POPs were higher than 95% (Table 1). The proportion of the trifunctional monomer to the bifunctional monomer was kept at a 2:3 M ratio. As an example, the synthesis of the TRP-MeIS (POP2) is described as follows:

An oven-dried, 50 mL three-necked Schlenk flask equipped with a mechanical stirrer was charged with triptycene (3.49 g, 13.8 mmol), MeIS (3.35 g, 20.8 mmol) and $CHCl_3$ (15 mL). The mixture was stirred at room temperature under a nitrogen blanket until the monomers reached complete dissolution. The flask was then cooled to 0 °C and trifluoromethanesulfonic acid (30 mL) was slowly added for 15–20 min using an addition funnel. The reaction mixture was allowed to warm to room temperature and stirred for 5 days. The product was poured into a water/ethanol mixture (3:1), filtered, and consecutively washed with water, acetone, chloroform, and again with acetone. The product was then dried in a vacuum oven at 150 °C for 12 h. The observed yield was 97%.

2.4. Membrane preparation

Membranes were prepared using the polymers from 10% (w/v) solutions. All solutions were filtered through a Symta® glass-fiber filter with a pore size of 3.1 μm and carefully spread on a leveled glass plate at 30 °C (60 °C when the solvent used was DMAc). The solvent was then allowed to evaporate at this temperature for 12 h, and then at 60–80 °C for another 12 h. Finally, the membranes were subjected to a series of thermal treatments in a vacuum oven: 80 °C/30 min, 100 °C/1 h, 120 °C/30 min, 150 °C/1 h, and 180 °C/12 h. Homogeneous films were obtained with thickness values between 40 and 60 μm.

To prepare the MMMs with POPs loadings of about 20% w/w (relative to the polymer weight), the POP filler was previously heated at 180 °C in a vacuum oven and stored under vacuum. Some polymer networks (POP1 and POP2) were CO_2 plasma treated to modify their surface, with the idea of improving the interfacial compatibility between the polymer matrix and the filler. Details of the plasma treatment are given in the characterization methods section.

As an example, the preparation of a MMMs is described as follows:

A suspension of POP (100.0 mg) in 4 mL of $CHCl_3$ was stirred for 24 h at room temperature, followed by sonication for 20 min with a 130 W ultrasonic probe (Vibra Cell 75186) operating at 50% of its maximum amplitude. The procedure consisted of 40 cycles where the ultrasound (US) source was 20 s *on* and then 10 s *off*. It was observed that these US cycles achieved an excellent dispersion of the particles. Then, 1.5 mL of a filtered polymer solution (600 mg of polymer in 4.0 mL of $CHCl_3$) was added to the suspension with stirring. The suspension was sonicated for 2 min before adding the rest of the polymer solution and stirring for 10

Table 1
Reaction yield and porosity parameters of POPs.

Acronyms	Yield[a,b]	S_{BET}[c]	V_{total}[d]	V_{micro}[e]	Microporosity[f] (%)
TRP-IS: POP1	>95	867	0.50	0.31	62
TRP-MeIS: POP2	>95	866	0.55	0.31	56
135TPB-IS: POP3	>95	1033	0.64	0.37	58
135TPB-MeIS: POP4	>95	906	0.55	0.32	58

[a] The reaction was maintained at room temperature for 1 h, and 60 °C for 96 h.
[b] Reaction yield (%).
[c] Specific surface area ($m^2\ g^{-1}$).
[d] Total pore volume ($cm^3\ g^{-1}$).
[e] Micropore volume ($cm^3\ g^{-1}$).
[f] Microporosity = 100x (V_{micro}/V_{total}).

min. The films of MMMs were cast following the procedure described above for linear polymers.

The polymer acronyms are shown in Table S1 in section 2 of supporting information.

2.5. Characterization methods

^{1}H and ^{13}C nuclear magnetic resonance (NMR) spectra were collected on a Bruker Avance 400 MHz or an Agilent MR-500 MHz spectrometer. Samples were prepared at 30 $mgml^{-1}$ using $CHCl_3$-d or DMSO-d_6. Attenuated total reflectance-Fourier Transform Infrared (ATR-FTIR) spectra were collected on a PerkinElmer Spectrum spectrometer.

POPs porosity was characterized via N_2 adsorption−desorption isotherms measured at −196 °C (77 K) using an ASAP 2010 device (Micromeritics). The relative pressure (P/P_0) varied from 10^{-6} to 0.995. The minimum equilibrium time (both for the adsorption and desorption) was 300 s. Before testing, samples were degassed at 125 °C for 18 h under vacuum to remove any absorbed humidity or other gases. The adsorption branch of the isotherms was used to obtain the apparent surface area (S_{BET}) by applying the Brunauer− Elmmett−Teller method for P/P_0 from 0.01 to 0.2 and for a micropore volume (V_{micro}) (using the Dubinin−Radushkevich (DR) equation) from 0.001 to 0.2 of relative pressure. The total pore volume (V_{total}) was found from the volume of liquid nitrogen adsorbed at 0.975 relative pressure.

Thermogravimetric analysis (TGA) was performed on a TG-Q500 analyzer, using nitrogen gas flow (60 mL/min). The samples were heated at 20 °C/min from 30 to 850 °C using the Hi- Res method, with sensitivity and resolution parameters of 1 and 4.

Differential scanning calorimetric (DSC) analysis was run using on a DSC Q-2000 Analyzer (TA Instruments). Experiments were conducted using approximately 6 mg of sample in hermetic aluminum pans at a heating rate of 20 °C min^{-1} under nitrogen. DSC thermograms were collected from 50 °C to 375 °C.

Wide angle X-ray scattering (WAXS) patterns were recorded using a Bruker D8 Advance diffractometer equipped with a Goebel Mirror and a PSD Vantec detector in the reflection mode at 30 °C. The scattering angle, 2θ, was measured between 3 and 60°.

The solubility of the polymers was tested with different solvents in a test tube (1–2 mg of polymer in 0.1 mL of solvent). Each solution was magnetically stirred for 24 h. If the polymer sample did not dissolve after 24 h, it was heated to the boiling point of the solvent, and solubility was checked.

Inherent viscosities were measured at 30 °C using a Lauda iVisc device and an Ubbelohde viscometer. The viscosities were measured using $CHCl_3$ or DMAc as solvents, at 0.5 g dL^{-1} concentration.

Polymer density (ρ) was determined using a top-loading electronic XS105 Dual Range Mettler Toledo balance which is coupled with a density kit operating on Archimedes' principle. The samples were sequentially weighted in air and in high purity isooctane at room temperature. The density was calculated from the following equation (1):

$$\rho = \rho_{liquid} \times \frac{w_{air} - w_{liquid}}{w_{air}} \quad (1)$$

where ρ_{liquid} is the density of isooctane, w_{air} is the weight of the sample in air and w_{liquid} is its weight when it was submerged in isooctane. Four density measurements were run for each sample.

The density data were used to evaluate chain packing using the fractional free volume (FFV), which was calculated using the following equation (2):

$$FFV = \frac{V_e - 1.3V_w}{V_e} \quad (2)$$

where V_e is the polymer specific volume and V_w is the van der Waals volume. Molecular modeling of the polymer repeating units was run using the semiempirical Austin Model (AM1) in the Biovia Materials Studio program [34]. The optimized repeating units were then used to determine the molecular volume by constructing a 20-unit polymer structure using the Builder Polymers and Atom Volumes and Surface algorithms.

Computer simulations were carried out by first drawing the molecules in Hyperchem [35] and then optimizing the molecular and intermediate structures at the AM1 level [36]. Subsequently, electronic energies of the optimized geometries were calculated by density functional theory (DFT) (without any geometrical constraint (use of Opt keyword) for starting molecules and final molecules) using the Becke's three-parameter hybrid function with the 6-31G (d,p) basis set (B3LYP/6-31G (d,p)) [37] by means of the Gaussian 09 program [38, 39]. Molecular depictions were created using the Gaussview 5 program [40].

DF protonation (mono- or di-) was determined by calculating the DFTB3LYP/6-31G (d,p) electronic energies of a DF model and their protonated moiety (Scheme S1, section 12 SI). It was observed that the first protonation of DF model was highly exoergic (−72.2 kcal/mol), while the second one was endoergic (20 kcal/mol). Therefore, in the calculations of atomic volumes it was considered that the protonated form of DF polymers was DF-1H.

Scanning electron microscopy (SEM) images were taken with a Philips XL-30 ESEM on Au–Pd metalized samples operating at an acceleration voltage of 25 kV in high vacuum. The samples were cryo-fractured in liquid nitrogen. Mechanical properties were evaluated under uniaxial tensile tests at room temperature using an MTS Synergie-200 testing machine equipped with a 100 N load cell. Pneumatic clamps were used, and an extension rate of 5 mm/min was applied with a gauge length of 10 mm.

Some MMMs were prepared using POPs previously subjected to a CO_2-plasma surface treatment to test the possible effect of this treatment on the filler compatibility with the polymer matrix, and consequently, on gas transport properties. The CO_2-plasma surface treatment of the POP was carried out on 1.0 g of the material using a Harrick PDC-002 plasma-cleaner device, where the sample was positioned in the medium of the quartz plasma cylinder and treated for 30 min. The operating radio-frequency power was kept at 10 W (medium position), and the chamber pressure was kept at 200–250 Torr with a CO_2 flow of 25 mL/min.

2.6. Gas transport properties

He, O_2, N_2, CH_4 and CO_2, permeability was measured at 35 °C using a constant volume barometric device, with a feed upstream pressure of 3 bar. Prior to the measurements, the membrane was maintained under vacuum for about 12 h to remove any trace of humidity or residual solvent. Then, a pressure of 3 bar was applied to the membrane and the increase in permeate pressure was recorded as a function of time.

Gas permeability was obtained from the following equation (3):

$$P = \frac{273,15}{76} \times \frac{Vl}{\pi r^2 T p_o} \times \frac{dp}{dt} 10^{10} \quad (3)$$

where V is the volume in cm^3 in the permeate compartment, l is the membrane thickness in cm, πr^2 is the membrane area in cm^2, T is the temperature in K, p_0 is the feed pressure in bar and dp/dt is the rate of pressure change in the downstream volume in units of mbar s^{-1}. P is expressed in barrer [1barrer = 10^{-10} (cm^3(STP) cm cm^{-2} s^{-1} $cmHg^{-1}$)]. Scalar factors are included to reference the molar flux at standard pressure and temperature (76 cmHg and 273.15 K). The permeability experimental uncertainty is about 10% based on standard deviations from 2-samples.

The ideal gas selectivity (or gas permselectivity), $\alpha_{A/B}$, for a pair of gases A and B was calculated from the gas permeability ratio:

$$\alpha_{A/B} = \frac{P_A}{P_B} \quad (4)$$

3. Results and discussion

3.1. Monomer reactivity

The synthetic methodologies described for making polymers derived from IS and MeIS were used for the ketone DF [11,41]. However, low molecular weight polymers were obtained [30]. Under these results, we proceeded to optimize the SEAr reaction for the DF monomer.

First, differential reactivity tests were performed to determine the relative kinetic rates for the formation of mono- and di-coupling of aromatic rings. Second, the competitive reactions between a mixture of two electrophile monomers (IS/MeIS or IS/DF) with an aromatic compound were studied.

The nucleophile of choice was fluorobenzene (FB) due to the ease of characterization of the complex reaction mixtures by NMR (^{1}H NMR, ^{13}C NMR, and ^{19}F NMR). It should be noted that FB produces a product mixture when reacted with activated ketones, in which >90% of the condensation reaction occurs at the 4-position (*para*-product) and <10% at the 2-position (*ortho*-product). Using ^{19}F NMR, the regioselectivity of the reaction could be easily assigned.

The differential reactivity study proceeded as follows:

T1 study. In a magnetically stirred flask placed in a bath at 35 °C, the electrophile monomer (IS, MeIS, or DF) and TFSA (TFSA/electrophile, 10 mol/1 mol) were mixed with an equimolar amount of FB (FB/electrophile, 1 mol/1 mol) in $CHCl_3$ ($CHCl_3$/electrophile, 5 mol/1 mol). After 24 h, the reaction mixture was poured into water (pH = 8, using $NaHCO_3$). The aqueous portion was extracted three times with $CHCl_3$, and the combined $CHCl_3$ solutions were dried with $MgSO_4$, filtered, and concentrated in a rotary evaporator. The organic reaction products were analyzed by ^{1}H NMR,^{13}C NMR and ^{19}F NMR spectroscopy (NMR spectra are shown in Section 4 of the supporting information section).

It was observed that the electrophilic monomer was always present in the reaction product mixture. More interestingly, no NMR peaks associated to the mono-coupled entity 1 (Fig. 1) were observed (within the sensitivity of NMR). It seems logical to think that as soon as entity 1 is formed, the reaction progresses rapidly towards entity 2, leading to the total formation of the di-coupled compound.

T2 study. An equimolar mixture of electrophile monomers (IS/MeIS or IS/DF, 1 mol/1 mol) was placed in a reaction batch at 35 °C. FB was added in equimolar ratio to the total number of electrophiles (FB/electrophile, 2 mol/1 mol). (The same synthetic methodology for the T1 study was employed). Characterization of the reaction mixture was performed by ^{1}H NMR,^{13}C NMR and ^{19}F NMR spectroscopy.

A molar ratio of almost 1:1 of di-coupled compounds was observed for the IS/MeIS reaction, while for the IS/DF monomer mixture the amount of di-coupled IS compound was much higher (around 4–5 times) than that of the di-coupled DF compound.

Therefore, it could be stated that.

a) The reaction for these three monomers (IS, MeIS and DF) with FB led exclusively to the formation of the di-coupled derivative (entity 2 of Fig. 1).

b) IS and MeIS showed similar reactivity with FB, much higher than that of DF. Thus, the reactivity scale found for these three electrophilic monomers was as follows: IS ≥ MeIS >DF.

Due to the clear kinetic differences between the first reaction (i.e., reaction of the ketone with the aromatic ring) and the second one (i.e., reaction of the formed hydroxy derivative with the other aromatic ring), it is possible to obtain linear, non-cross-linked polymers using non-stoichiometric conditions [30]. Thus, reaction tests at 5 °C were carried out for the formation of DF polymers using an excess of electrophile (5% molar excess). Using this non-stoichiometric methodology, the formation of a high-viscosity solution was achieved in a short reaction time (a few hours). However, all reactions produced a certain degree of cross-linking, which made it difficult to know at what time these reactions should be stopped. Therefore, it was considered convenient to use a stoichiometric Carothers methodology at 5 °C for long times. This modification produced soluble, high molecular-weight polymers by maintaining the reaction for 10–12 days..

The synthesis scheme of polymers, and copolymers, is shown in Fig. 2. The chemical structures of POPs are shown in Fig. 3.

The apparent surface area (S_{BET}), the micropore volume (V_{micro}), and the total pore volume (V_{total}) of POPs were studied. The porous polymer networks exhibited S_{BET} values between 800 and 1000 $m^2\ g^{-1}$. The S_{BET} values are listed in Table 1 while the N_2 adsorption/desorption isotherm graphs can be found in Fig. S47 of the supporting information.

To obtain MMMs, the polymer BP-IS was combined with POP1 and POP3 (polymer networks derived from IS, Fig. 3), whilst the polymer BP-MeIS was combined with POP2 and POP4 (polymer networks derived from MeIS, Fig. 3).

3.2. Characterization of polymers and membranes

Polymers were characterized by ^{1}H Nuclear Magnetic Resonance (^{1}H NMR) and ^{13}C Nuclear Magnetic Resonance (^{13}C NMR) using DMSO-d_6 or chloroform-d/TFA (for DF polymers) as solvents. As an example, the ^{1}H NMR spectrum of the linear polymer BP-IS is shown in Fig. 4, (NMR spectra are provided in section 3, SI).

BP-IS; ^{1}H NMR (500 MHz, DMSO-d_6): δ_H (ppm); 10.80 (s, 1H), 7.57 (d, J = 8.3 Hz, 4H), 7.26 (m, 6H), 6.98 (m, 2H)·^{13}C NMR (101 MHz, DMSO-d_6): δ_c (ppm) = 178.42, 141.87, 141.49, 138.96, 133.37, 129.07, 127.26, 62.18.

Polymer solubility was tested in methane sulfonic acid (MSA), N,N-dimethylacetamide (DMAc), N-methyl-2-pyrrolidinone (NMP), formic acid, $CHCl_3$, and a mixture of $CHCl_3$ and TFA (10% w/w TFA/$CHCl_3$). As shown in Table S2 (Section 7, SI), the homopolymers derived from IS and MeIS easily dissolved in aprotic polar solvents, while those derived from DF did not. BP-DF homopolymer and their copolymers only dissolved in acidic solvents (BP-DF and BP-DF-MeIS were soluble in formic acid and MSA, whilst BP-DF-IS was only soluble in a mixture of chloroform and TFA). Therefore, BP-DF, BP-DF-IS, and BP-DF-MeIS films were obtained in the protonated form (i.e., the bipyridine moiety was protonated in the solvent) and therefore an additional deprotonation step had to be performed by immersing the polymeric films in basic water (pH = 9) for 24 h. Both protonated and deprotonated membranes were tested in this work. The protonated films have been denoted by

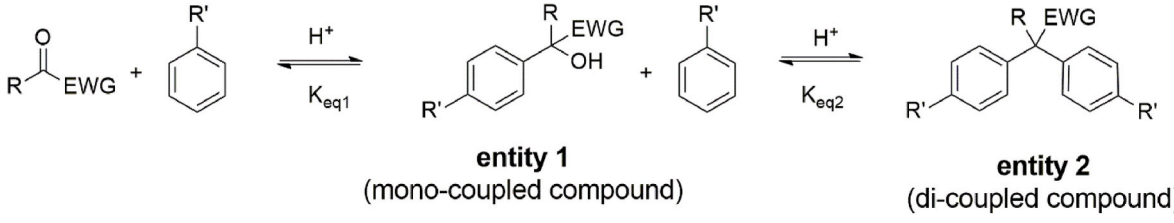

Fig. 1. T1 reactivity scheme.

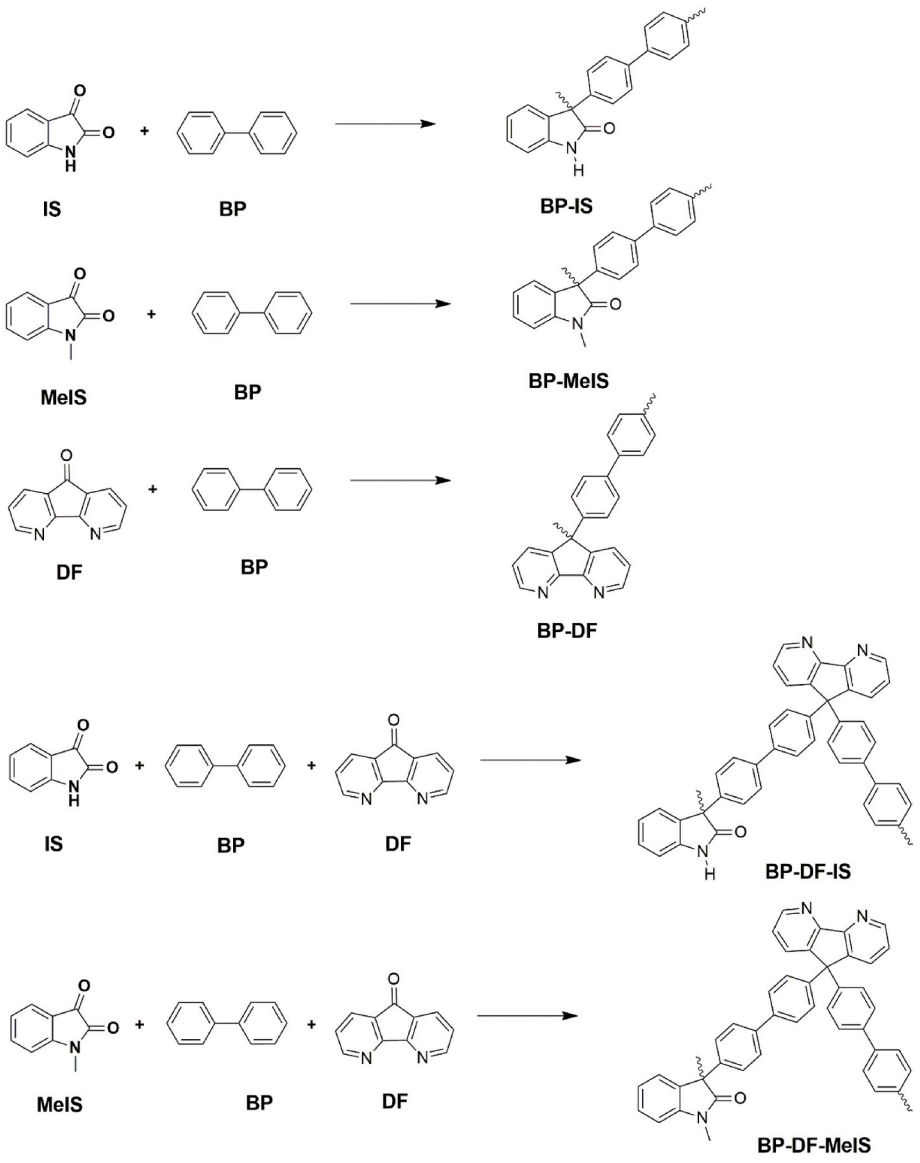

Fig. 2. Synthesis of polymers and copolymers.

adding "pt" to the end of the nomenclature.

Viscosity values of the polymers that could be dissolved in non-acidic solvents were determined. The results are provided in Table S3, section 8, SI. Since polymers were not soluble in the same solvent, their viscosities values could not be compared. It should be noted that although the viscosity of BP-DF-MeIS in $CHCl_3$ is low, this polymer gave membranes with mechanical properties good enough to permit its testing as a gas separation material.

Neat polymer membranes and MMMs were characterized by ATR-FTIR. The neat linear polymer spectra are shown in Fig. 5. FTIR spectra of BP-IS exhibited the characteristic bands of the 5-member lactam rings at 3390 (N–H st), 1710 (C═O st), and 1600 (N–H δ) and the typical bands at 1610, 1495 and 1470 cm^{-1} assigned to stretching vibrations of aromatic carbons (C_{ar}–C_{ar} st). In the case of the FTIR spectrum of BP-MeIS, the previous two bands related to the N–H bond did not appear and the band at 1495 cm^{-1} increased in intensity due to its overlapping with the bending vibration of methyl groups (CH_3 δ). The BP-DF spectrum showed a characteristic band at 1400 cm^{-1}, which was assigned to the bending vibration of C_{ar}–H bond (C_{ar}–H δ) of the bipyridine moiety [17]. In the case of the copolymers, the characteristic IR bands of DF and IS or MeIS were identified according to their chemical structure.

The ATR-FTIR spectra of MMMs are displayed in Figs. S40 and S41 (section 10.1, SI). The spectra of MMMs were compared with those corresponding to neat linear polymers. Unfortunately, since POPs and linear polymers share the same functional groups (lactam rings), accurate FTIR characterization was not possible.

The WAXS patterns of the SEAr polymer membranes are shown in Fig. 6. All of the membranes showed an amorphous halo with at least three main intensity maxima appearing approximately at 2θ: 12.2, 16.4, and 22.0°. The most probable intersegmental distances (d) in the polymer chains' packing were determined from the Bragg's equation ($\lambda = 2d\sin\theta$), and thus, three intersegmental distances were obtained from the position of the maximum: 0.72, 0.54 and 0.40 nm. The shape of the patterns of the membranes indicated that the contribution of the largest distances to the amorphous halo was higher for BP-MeIS, followed by BP-IS and then BP-DF. This result could be related to the fact that the MeIS moiety would introduce more FFV than IS and DF ones. On the other hand, the addition of POP particles to the polymer matrix did not cause significant change in the patterns of MMMs relative to the corresponding neat membranes, as seen in Fig. S44 for BP-IS and BP-MeIS based membranes (graphics are provided in section 10.3, SI).

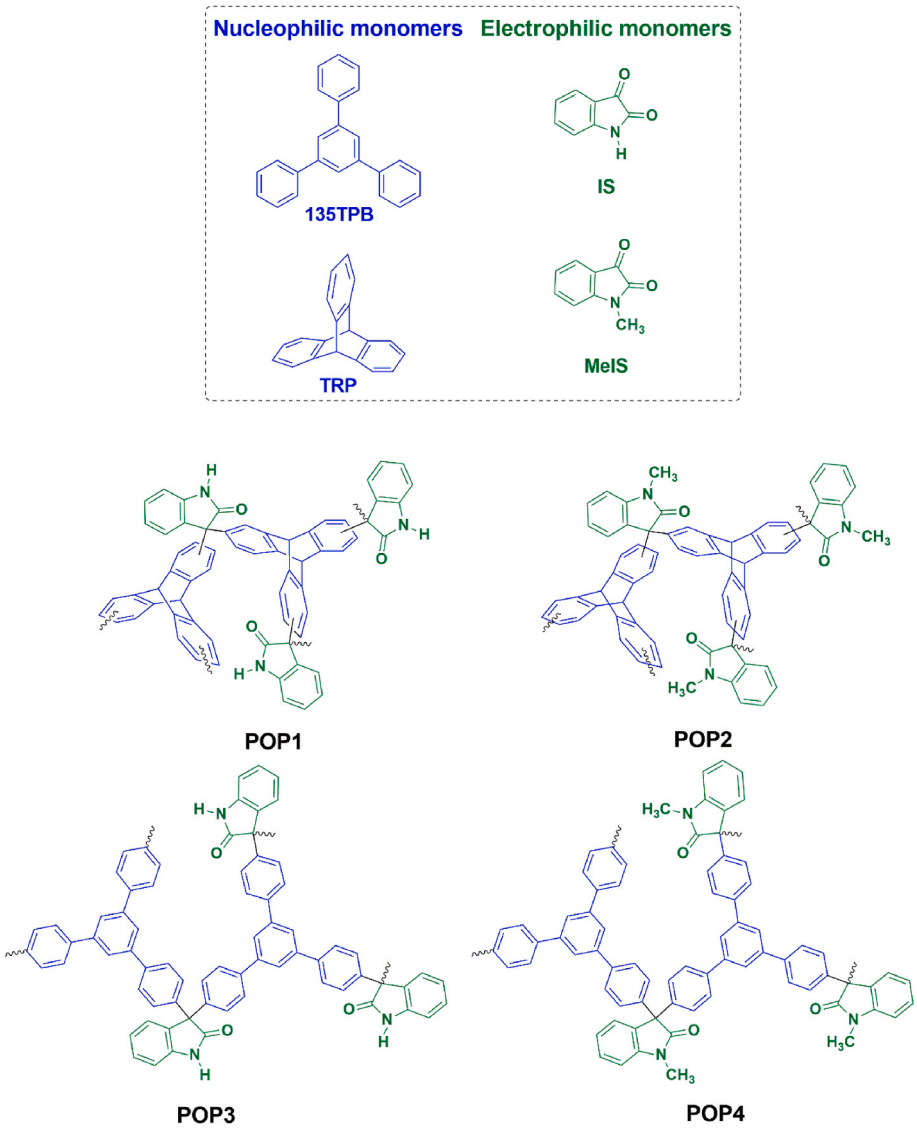

Fig. 3. Chemical structures of POPs.

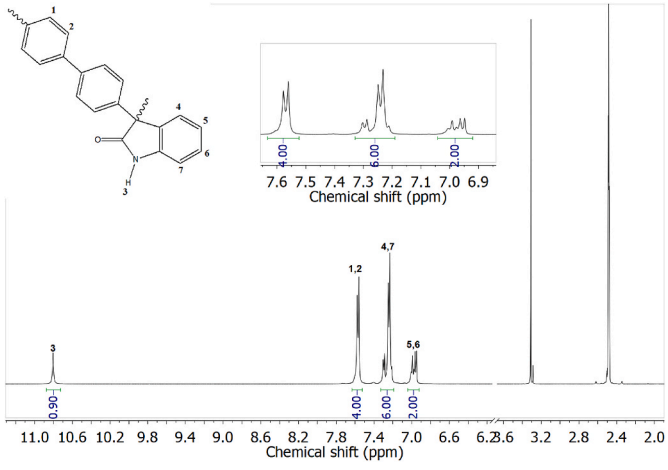

Fig. 4. ^{1}H NMR spectrum of BP-IS (DMSO-d_6).

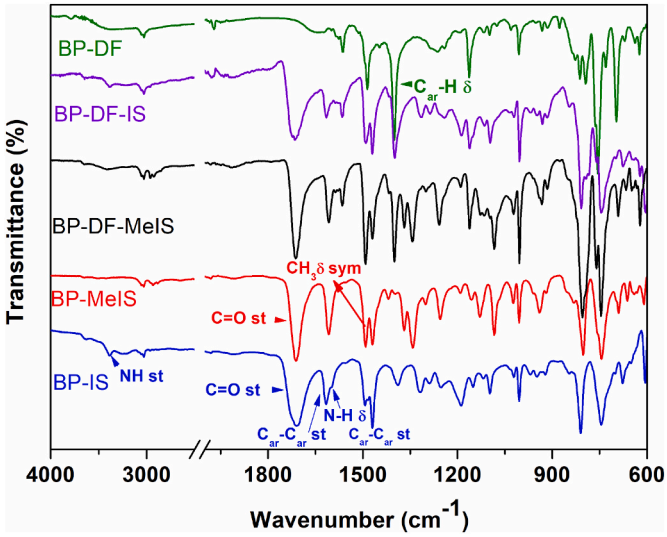

Fig. 5. ATR-FTIR spectra of linear polymers.

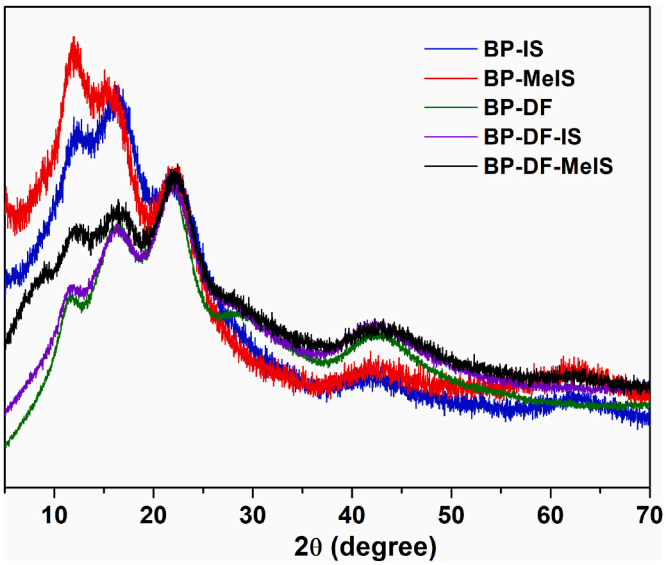

Fig. 6. WAXS patterns of membranes (curves were normalized to the maximum that appears at 22°).

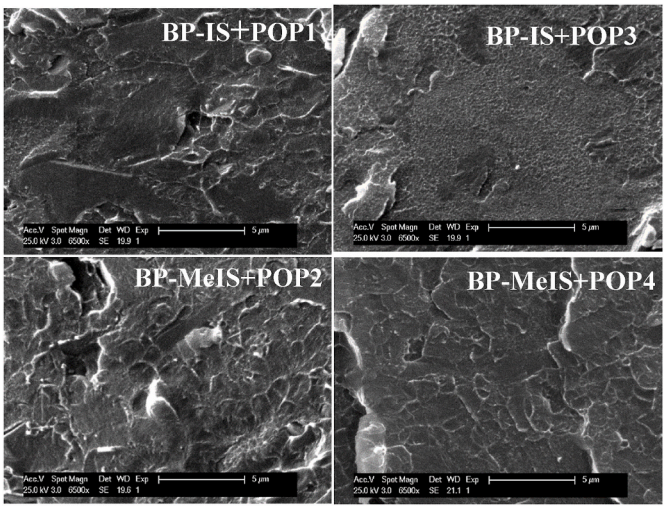

Fig. 7. SEM micrographs of the cross-section of MMMs.

MMMs cross-sections were characterized *via* electron microscopy (SEM) (cf. Fig. 7). The morphologies of MMMs from POPs having 135TPB (POP3 and POP4) revealed a more homogeneous dispersion of the POP particles than those from triptycene-based POPs (POP1 and POP2), suggesting better compatibility between polymer matrix and filler. Furthermore, BP-MeIS + POP4 showed a smooth homogeneous morphology in which neither agglomerates nor particles were distinguished, which may be due to the presence of very small POP particles.

The mechanical properties of pure polymer and MMM films (tensile strengths, Young's module, and elongations at break) at room temperature are listed in Table S5 (section 10.4, SI). The addition of POP in the BP-IS polymer matrix caused an increase (1.3 times) in Young's modulus and a slight reduction in elongation at break (1.07 and 1.53 times for POP1 and POP2 respectively). This embrittlement is most likely caused by small defects in the membranes produced by the presence of small POP agglomerates or by cracking caused by the cutting of the probes [19]. It was observed that the deprotonation of DF polymers did not decrease their mechanical resistance.

DSC thermogram (cf. Fig. S39, Section S6.6, SI) showed that most of the polymer films did not exhibit any transition up to 375 °C. For the protonated membranes, an endothermic peak below 250 °C is visible, which is associated with the deprotonation of the bipyridine group.

The thermal stabilities of neat polymers, porous polymer networks, and MMM films were studied via dynamic TGA under a nitrogen purge (Figs. 8 and 9 and S42-S43, supporting information). The first weight loss below 150 °C was related to the desorption of humidity from the material. The second weight loss, between 250 and 400 °C, of the MMMs could be associated with residual solvent trapped in the membrane. The weight loss above 500 °C was associated to the polymer degradation.

3.3. Thermal and chemical stability of SEAr-derived polymeric membranes

An isothermal TGA study up to 450 °C was performed to test the thermal stability of these polymeric materials in long-term applications. Chemical stability was determined by placing the films in very low and very high pH solutions; changes in chemical structure, if any, were checked by ATR-FTIR.

(a) ***Isothermal TGA study.***

In this case, the film samples were studied using the following isothermal TGA program:

250 °C/30min (to dry the samples and remove solvent and other residues)//350 °C/60min.//450 °C/60 min.

Isothermal TGA (Fig. 10 and S32-S38, included in section 6, SI) revealed weight losses before 300 °C (weight losses due to the solvent and water trapped in the material). Between 350 °C and 450 °C, the isothermal weight losses for all the polymer matrixes and MMMs did not exceed 2%.

Therefore, it can be stated that the thermal stability of these materials is excellent.

(b) ***Chemical stability study***

Membrane samples were immersed in two solutions, one at pH = 10 (potassium hydroxide solution) and another at pH = 2 (hydrochloric acid solution). These solutions were refluxed for 48 h and subsequently, the samples were collected and repeatedly washed in hot distilled water. Finally, they were dried at 180 °C (as described in Section 5, SI) and ATR-FTIR was performed. It should be noted that for the DF-derived membranes, the acid treatment of the membranes resulted in protonation of the bipyridine groups, so the samples were treated in a basic solution (pH = 8) for 30 min to deprotonate them.

The polymers are mostly composed of aromatic moieties linked by non-labile bonds, (the only labile groups could be the lactam groups present in the IS- and MeIS-derived structures). In a previous work, it

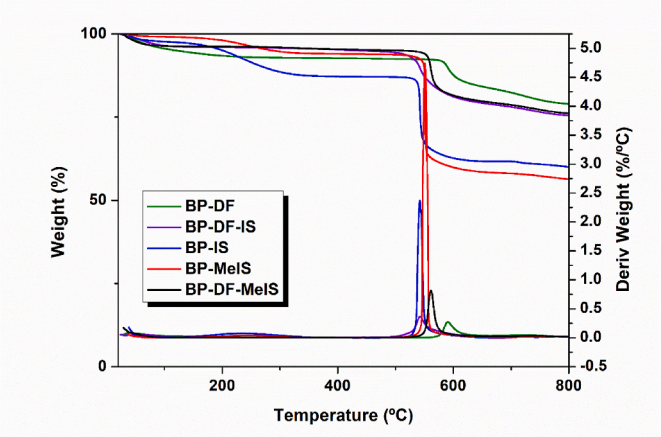

Fig. 8. TGA of linear polymer films.

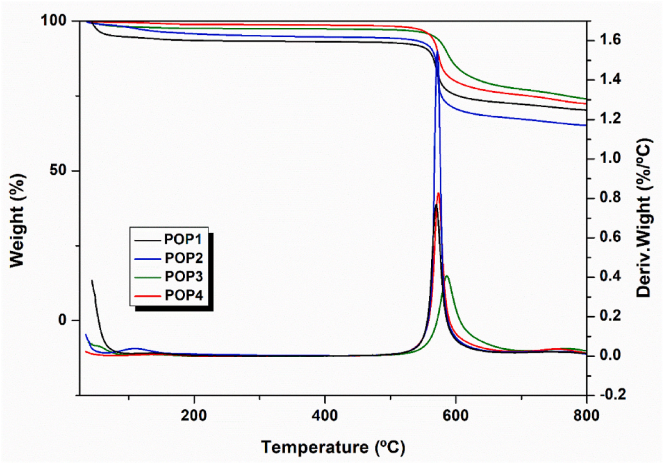

Fig. 9. TGA of porous polymer networks.

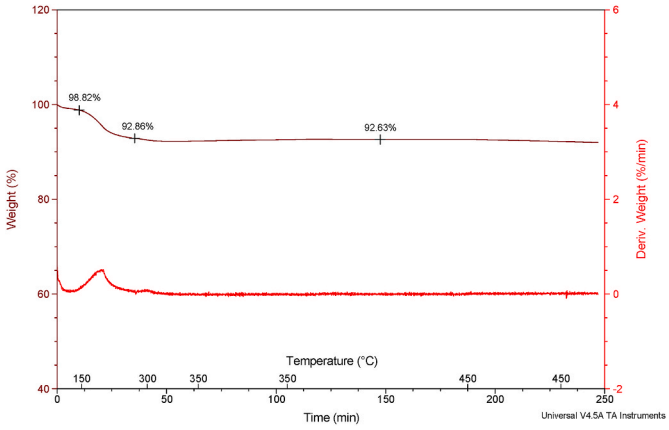

Fig. 10. Isothermal TGA plot of BP-MeIS + POP2.

was observed that these lactam units present in porous polymer networks were chemically stable [16]. This fact could be explained by the extraordinary rigidity of these materials, which makes the opening of the lactam thermodynamically unfavorable. If the opening were to occur, the lactam units would be restored during the drying phase [16].

The FTIR analysis (Figs. S27–S31) in the supplementary information section shows that the acid treatment did not produce any significant change in the polymer's structure, i.e., FTIR spectra of these films matched that of the non-treated membranes. Noteworthy, the FTIR of DF polymer films that were not neutralized after the acid treatment coincided with the FTIR of the protonated DF polymer films.

For polymers treated in very basic solutions (Fig. in section 5, SI), no significant differences were observed in the FTIR plots for the homopolymer derived from DF after drying at 180 °C.

The basic treatment broadened the FTIR absorbances between 3750 and 2500 cm^{-1} when the drying treatment was not performed on homopolymers and copolymers derived from IS and MeIS. However, all cast membranes treated at 180 °C showed quite similar FTIR fingerprints.

In conclusion, we can state that these polymer materials exhibit excellent chemical and thermal stability.

3.4. Gas transport properties

Pure gas He, O_2, N_2, CH_4, and CO_2 permeabilities and ideal O_2/N_2, CO_2/N_2, and CO_2/CH_4 selectivities are shown for each membrane in Table 2.

The gas permeability for the homopolymer membranes decreased in the following order: BP-MeIS > BP-DF > BP-IS. The increase in permeability of BP-MeIS was higher for the largest gases than for the smallest ones; for instance, the increase in permeability was 3.94 times for CH_4 and 2.67 times for O_2, relative to BP-IS. This result is consistent with the higher FFV in the BP-MeIS membrane compared to BP-IS and BP-DF, as suggested by WAXS (Fig. 6). Relative to the BP-IS membrane, BP-MeIS and BP-DF showed CO_2 permeability about 1.75 times higher than He. This fact is usually observed in high FFV materials [42–46].

The protonation of the bipyridine moiety considerably increased the permeability of BP-DF; for instance, the permeability increase was 3.49 times for CH_4 and 2.63 times for O_2, when compared to the deprotonated form. In addition, the CO_2 permeability was 2.10 times higher relative to He permeability. In an attempt to explain the increase in permeability due to protonation of bipyridine moiety, the FFV was estimated from the bulk density of the membranes (the methodology used in the estimation of FFV is discussed in the characterization methods section. In that section, a DFT calculation is also included to justify that the bipyridine

Table 2
Permeability and ideal selectivity of homopolymer and copolymer membranes and MMMs at 3 bar and 30 °C. Uncertainties were calculated from multiple sample measurements [47].

Membrane	Permeability (barrer)					Selectivity		
Homopolymer	He	O_2	N_2	CH_4	CO_2	O_2/N_2	CO_2/N_2	CO_2/CH_4
BP-IS	40 ± 2	7.3 ± 0.3	1.41 ± 0.07	1.50 ± 0.08	42 ± 2	5.2 ± 0.3	30 ± 2	28 ± 2
BP-MeIS	67 ± 3	19.4 ± 0.6	4.5 ± 0.2	5.9 ± 0.3	120 ± 8	4.3 ± 0.2	27 ± 2	20 ± 2
BP-DF	49 ± 2	14.6 ± 0.7	3.2 ± 0.2	3.7 ± 0.2	86 ± 5	4.6 ± 0.4	27 ± 2	23 ± 2
BP-DF_pt	100 ± 3	38 ± 2	9.7 ± 0.5	13 ± 1	219 ± 13	3.9 ± 0.3	23 ± 2	17 ± 2
Copolymer	**He**	**O_2**	**N_2**	**CH_4**	**CO_2**	**O_2/N_2**	**CO_2/N_2**	**CO_2/CH_4**
BP-DF-IS	60 ± 3	14.7 ± 0.8	3.0 ± 0.2	3.4 ± 0.2	82 ± 5	4.9 ± 0.4	27 ± 2	24 ± 2
BP-DF-IS_pt	69 ± 3	18 ± 1	4.0 ± 0.2	4.8 ± 0.3	106 ± 7	4.5 ± 0.3	26 ± 2	22 ± 2
BP-DF-MeIS	63 ± 3	19 ± 2	3.8 ± 02	4.0 ± 0.4	97 ± 7	5.0 ± 0.6	26 ± 2	24 ± 3
BP-DF-MeIS_pt	63 ± 2	19 ± 2	3.8 ± 0.3	4.4 ± 0.4	100 ± 9	5.0 ± 0.7	26 ± 3	23 ± 3
MMM	**He**	**O_2**	**N_2**	**CH_4**	**CO_2**	**O_2/N_2**	**CO_2/N_2**	**CO_2/CH_4**
BP-IS + POP1	81 ± 3	13.6 ± 0.8	2.6 ± 0.2	3.1 ± 0.2	70 ± 4	5.2 ± 0.5	27 ± 3	23 ± 2
BP-IS + POP1_pl	49 ± 2	8.9 ± 0.5	2.0 ± 0.1	2.0 ± 0.1	44 ± 2	4.5 ± 0.4	22 ± 1	22 ± 1
BP-IS + POP2	20 ± 1	1.6 ± 0.2	0.359 ± 0.005	0.22 ± 0.03	7.4 ± 0.7	4.5 ± 0.6	21 ± 2	34 ± 6
BP-IS + POP2_pl	85 ± 2	21 ± 1	6.1 ± 0.4	5.1 ± 0.3	106 ± 6	3.4 ± 0.3	17 ± 2	21 ± 2
BP-IS + POP3	72 ± 2	17.5 ± 0.7	3.6 ± 0.2	4.0 ± 0.2	100 ± 5	4.8 ± 0.3	28 ± 2	25 ± 2
BP-MeIS + POP2	111 ± 1	38 ± 2	9.4 ± 0.5	12.4 ± 0.7	228 ± 12	4.0 ± 0.3	24 ± 2	18 ± 1
BP-MeIS + POP2_pl	67 ± 4	16 ± 1	4.3 ± 0.3	5.4 ± 0.4	81 ± 5	3.7 ± 0.3	19 ± 2	15 ± 1
BP-MeIS + POP4	84 ± 2	30 ± 2	7.4 ± 0.4	10.4 ± 0.6	200 ± 10	4.0 ± 0.3	27 ± 2	19 ± 1

unit undergoes only one protonation). The values obtained are listed in Table S4 in the supporting information section. However, this analysis was not conclusive since the membranes exhibited density and FFV that are within experimental error of each other.

As expected, the permeability values of the copolymer membranes, BP-DF-IS and BP-DF-MeIS were between their two homopolymer membrane counterparts. In contrast to what was observed for BP-DF, protonation of the bipyridine moiety in the copolymer membranes BP-DF-IS_pt and BP-DF-MeIS_pt did not cause significant changes in permeability, relative to their deprotonated form.

Overall, the MMMs showed higher permeabilities than the pristine polymeric membranes, with no significant change in selectivity.

Unexpectedly, the BP-IS + POP2 membrane, which incorporated the POP derived from MeIS (POP2), showed a gas permeability that was 80% lower relative to the BP-IS-based MMMs. It was considered that this anomalous result might be due to undesirable effects such as polymer chain rigidification and partial pore blockage. In previous research, analogous POPs were modified by using a CO_2-plasma treatment to make their surfaces more hydrophilic, and it was seen that the gas separation properties of the corresponding MMMs were improved [20]. In an attempt to overcome this drawback, the surfaces of POP1 and POP2 were modified using the same plasma treatment, and BP-IS + POP1_pl, BP-IS + POP2_pl, and BP-MeIS + POP2_pl MMMs were prepared. However, the results were not evident, as the gas permeability of BP-IS + POP1 and BP-MeIS + POP2 (MMMs derived from the POPs sharing the ketone group with the polymer matrix) was reduced by 0.60–0.77 and 0.36–0.45 times, respectively, after the CO_2-plasma treatment. However, the permeability of the BP-IS + POP2 was increased for all of gas types, especially for CH_4 gas (23-folder higher after the plasma treatment).

The permeability was decomposed in its elementary diffusivity and solubility contributions using the time-lag analysis discussed in section 11.2 of the SI. Tables S6 and S7 (supporting information section 11.2) summarize the diffusivity and solubility coefficients for all membranes. The diffusivities of BP-MeIS and BP-DF_pt were higher than those of BP-IS and BP-DF. Similar to permeability, the increase in diffusivity was higher for larger gases. Thus, the ideal selectivity seems to be controlled mainly by the diffusivity selectivity. In the case of the MMMs, diffusivity also showed the largest contribution to permeability and was somewhat higher for the membranes derived from BP-IS-derived membranes.

The gas separation performance for neat linear polymers and MMMs were compared to other standard polymers used in gas separation membranes (i.e., Matrimid and PPO). The results are shown in the Robeson diagrams for several gas pairs: CO_2/CH_4 in Fig. 11, CO_2/N_2 in Fig. S45, and O_2/N_2 in Fig. S46. Both the 1991 and 2008 Robeson upper bounds are included [48,49]. In general, it was observed that the use of a POP load led to an increase in permeability (between 50 and 100%). For CO_2/CH_4 and O_2/N_2 gas pairs, the MMMs were closer to the 1991 Robeson upper-bound. For the CO_2/N_2 gas pair, the selectivity was quite similar for both neat polymer membranes and MMMs.

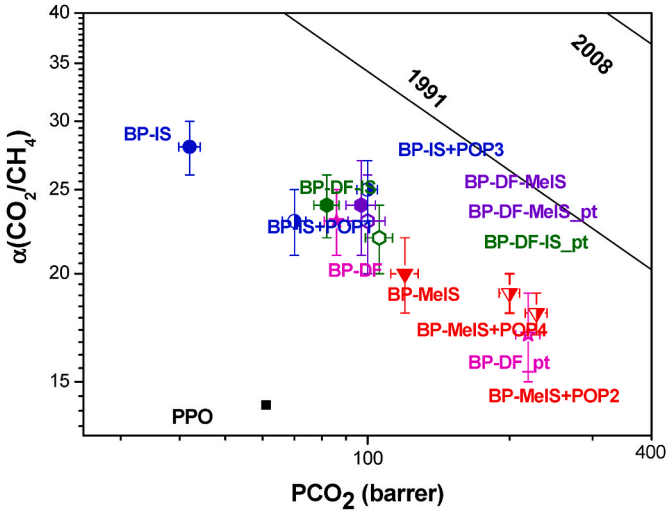

Fig. 11. CO_2/CH_4 Robeson diagram for neat polyimide and copolyimide membranes and MMMs. Solid lines represent the 1991 and 2008 upper bounds Data for reference polymer used in gas separation were taken from Ref. [50]: Matrimid and poly (phenyl oxide) (PPO). The standard deviations from repeated measurements are shown as error bars.

4. Conclusions

A new set of gas separation polymer materials was prepared *via* the hydroxyalkylation reaction (SEAr) between biphenyl, and ketones containing electron-withdrawing groups (isatin, IS; N-methylisatin, MeIS, and 4,5-diazafluoren-9-one, DF). Since these polymers have no labile groups, they exhibited high chemical stability under very acidic or basic conditions.

Mixed matrix membranes (MMMs) were prepared by combining these linear polymers with porous organic polymers (POPs) having a similar chemical structure. The MMMs showed good compatibility and mechanical properties. All of these materials exhibited thermal stability above 450 °C and no glass transition temperature below 375 °C.

Both the neat polymer/copolymer membranes and MMMs were tested in gas separation applications. In general, the gas separation productivity of both pristine polymers and MMMs was good. For the homopolymer derived from DF, protonation of the bipyridine increased gas permeability with a slight reduction in selectivity. For MMMs derived from MeIS, CO_2 permeability values higher than 200 barrer were achieved.

Finally, the combination of a linear polymer (BP-IS) and a POP derived from MeIS (POP2: TRP-MeIS) resulted in an inhomogeneous MMM with poor gas separation properties. This drawback was alleviated by treating the POP using CO_2 plasma. After plasma treatment, the gas separation properties improved.

Funding sources

This work was supported by Spain's Agencia Estatal de Investigación (AEI) (Projects: PID2019-109403RB-C22 (AEI/FEDER, UE), PID2019-109403RB-C21 (AEI/FEDER, UE) and PID2020-118547 GB-I00 (AEI/FEDER, UE)) and by the Spanish Junta de Castilla y León (VA224P20). M.T.W. and M.G. acknowledge partial financial support from the US National Science Foundation (NSF) under the grant # 2005282.

CRediT authorship contribution statement

Laura Matesanz-Niño: Validation, Investigation, Formal analysis, Writing – original draft, Writing – review & editing. **Noelia Esteban:** Validation, Investigation, Formal analysis, Writing – review & editing. **Matthew T. Webb:** Validation, Formal analysis, Writing – review & editing. **Aránzazu Martínez-Gómez:** Investigation, Formal analysis, Writing – review & editing. **Fabián Suárez-García:** Validation, Investigation, Formal analysis. **Alfonso González-Ortega:** Validation, Methodology, Formal analysis, Supervision. **Jesús A. Miguel:** Validation, Formal analysis, Supervision, Funding acquisition, Writing – review & editing. **Laura Palacio:** Validation, Formal analysis, Supervision, Funding acquisition. **Michele Galizia:** Methodology, Resources, Writing – original draft, Writing – review & editing, Funding acquisition. **Cristina Álvarez:** Conceptualization, Methodology, Resources, Supervision, Writing – original draft, Writing – review & editing. **Ángel E. Lozano:** Conceptualization, Methodology, Resources, Writing – original draft, Writing – review & editing, Funding acquisition.

Declaration of competing interest

The authors declare that they have no known competing financial interests or personal relationships that could have appeared to influence the work reported in this paper.

Data availability

No data was used for the research described in the article.

Acknowledgments

The authors acknowledge Salvador Azpeleta for the WAXS measurements taken at the LTI Facilities of the University of Valladolid.

L.M.N. thanks the University of Valladolid for UVa-2019 and UVa-2021 mobility grants.

Appendix A. Supplementary data

Supplementary data to this article can be found online at https://doi.org/10.1016/j.polymer.2022.125647.

References

[1] W.H. Carothers, Polymers and polyfunctionality, Trans. Faraday Soc. 32 (1936) 39, https://doi.org/10.1039/tf9363200039.
[2] W.H. Carothers, Studies on polymerization and ring formation. I. An introduction to the general theory of condensation polymers, J. Am. Chem. Soc. 51 (1929) 2548–2559, https://doi.org/10.1021/ja01383a041.
[3] W.H. Carothers, Polymerization., Chem. Rev. 8 (1931) 353–426, https://doi.org/10.1021/cr60031a001.
[4] S. Ramakrishnan, Condensation polymerization, Resonance 22 (2017) 355–368, https://doi.org/10.1007/s12045-017-0475-0.
[5] O. Hernández-Cruz, M.G. Zolotukhin, S. Fomine, L. Alexandrova, C. Aguilar-Lugo, F.A. Ruiz-Treviño, G. Ramos-Ortíz, J.L. Maldonado, G. Cadenas-Pliego, High- T g functional aromatic polymers, Macromolecules 48 (2015) 1026–1037, https://doi.org/10.1021/ma502288d.
[6] L.I. Olvera, M.T. Guzmán-Gutiérrez, M.G. Zolotukhin, S. Fomine, J. Cárdenas, F. A. Ruiz-Trevino, D. Villers, T.A. Ezquerra, E. Prokhorov, Novel high molecular weight aromatic fluorinated polymers from one-pot, metal-free step polymerizations, Macromolecules 46 (2013) 7245–7256, https://doi.org/10.1021/ma401306s.
[7] D.R. Nieto, M.G. Zolotukhin, L. Fomina, S. Fomine, Superacid mediated hydroxyalkylation reaction of 1,2,3-indanetrione: a theoretical study, J. Phys. Org. Chem. 23 (2010) 878–884, https://doi.org/10.1002/poc.1680.
[8] G.A. Olah, Superelectrophiles, Angew. Chemie Int. Ed. English. 32 (1993) 767–788, https://doi.org/10.1002/anie.199307673.
[9] G.A. Olah, D.A. Klumpp, Study of Superelectrophiles, in: Superelectrophiles Their Chem., John Wiley & Sons, Inc., Hoboken, NJ, USA, 2008, pp. 17–80, https://doi.org/10.1002/9780470185124.ch2.
[10] D.A. Klumpp, Superelectrophiles: charge–charge repulsive effects, Chem. Eur J. 14 (2008), https://doi.org/10.1002/chem.200701470, 2004–2015.
[11] M.C.G. Hernandez, M.G. Zolotukhin, S. Fomine, G. Cedillo, S.L. Morales, N. Fröhlich, E. Preis, U. Scherf, M. Salmón, M.I. Chávez, J. Cárdenas, A. Ruiz-Trevino, Novel, metal-free, superacid-catalyzed “click” reactions of isatins with linear, nonactivated, multiring aromatic hydrocarbons, Macromolecules 43 (2010) 6968–6979, https://doi.org/10.1021/ma101048z.
[12] R.R. Naredla, D.A. Klumpp, Contemporary carbocation chemistry: applications in organic synthesis, Chem. Rev. 113 (2013) 6905–6948, https://doi.org/10.1021/cr4001385.
[13] M.G. Zolotukhin, S. Fomine, L.M. Lazo, R. Salcedo, L.E. Sansores, G.G. Cedillo, H. M. Colquhoun, J.M. Fernandez-G, A.F. Khalizov, Superacid-catalyzed polycondensation of acenaphthenequinone with aromatic hydrocarbons, Macromolecules 38 (2005) 6005–6014, https://doi.org/10.1021/ma0503460.
[14] L.I. Olvera, F.A. Ruiz-Treviño, J. Balmaseda, I.A. Ronova, M.G. Zolotukhin, M. P. Carreón-Castro, E. Lima, J. Cárdenas, R. Gaviño, Microporous polymers from superacid catalyzed polymerizations of fluoroketones with p-quaterphenyl: synthesis, characterization, and gas sorption properties, Polymer 102 (2016) 221–230, https://doi.org/10.1016/j.polymer.2016.09.021.
[15] M.O. González-Díaz, E. Cetina-Mancilla, R. Sulub-Sulub, A. Montes-Luna, L. I. Olvera, M.G. Zolotukhin, J. Cárdenas, M. Aguilar-Vega, Novel fluorinated aromatic polymers with ether-bond-free aryl backbones for pure and mixed gas separation, J. Membr. Sci. 606 (2020), 118114, https://doi.org/10.1016/j.memsci.2020.118114.
[16] B. Lopez-Iglesias, F. Suárez-García, C. Aguilar-Lugo, A. González Ortega, C. Bartolomé, J.M. Martínez-Ilarduya, J.G. de la Campa, Á.E. Lozano, C. Álvarez, Microporous polymer networks for carbon capture applications, ACS Appl. Mater. Interfaces 10 (2018) 26195–26205, https://doi.org/10.1021/acsami.8b05854.
[17] N. Esteban, M.L. Ferrer, C.O. Ania, J.G. de la Campa, Á.E. Lozano, C. Álvarez, J. A. Miguel, Porous organic polymers containing active metal centers for suzuki–miyaura heterocoupling reactions, ACS Appl. Mater. Interfaces 12 (2020) 56974–56986, https://doi.org/10.1021/acsami.0c16184.
[18] E.L. Vargas, N. Esteban, J. Cencerrero, V. Francés, C. Álvarez, J.A. Miguel, A. Gallardo, A.E. Lozano, M.B. Cid, Pyrrolidine-based catalytic microporous polymers in sustainable C N and C C bond formation via iminium and enamine activation, Mater. Today Chem. 24 (2022), 100966, https://doi.org/10.1016/j.mtchem.2022.100966.
[19] C. Aguilar-Lugo, F. Suárez-García, A. Hernández, J.A. Miguel, Á.E. Lozano, J.G. de la Campa, C. Álvarez, New materials for gas separation applications: mixed matrix membranes made from linear polyimides and porous polymer networks having lactam groups, Ind. Eng. Chem. Res. 58 (2019) 9585–9595, https://doi.org/10.1021/acs.iecr.9b01402.
[20] C. Aguilar-Lugo, W.H. Lee, J.A. Miguel, J.G. de la Campa, P. Prádanos, J.Y. Bae, Y. M. Lee, C. Álvarez, Á.E. Lozano, Highly permeable mixed matrix membranes of thermally rearranged polymers and porous polymer networks for gas separations, ACS Appl. Polym. Mater. 3 (2021) 5224–5235, https://doi.org/10.1021/acsapm.1c01012.
[21] C. Soto, E.S. Torres-Cuevas, A. González-Ortega, L. Palacio, P. Prádanos, B. D. Freeman, Á.E. Lozano, A. Hernandez, Hydrogen recovery by mixed matrix membranes made from 6FCl-apaf HPA with different contents of a porous polymer network and their thermal rearrangement, Polymers 13 (2021) 4343, https://doi.org/10.3390/polym13244343.
[22] C. Soto, E.S. Torres-Cuevas, A. González-Ortega, L. Palacio, Á.E. Lozano, B. D. Freeman, P. Prádanos, A. Hernández, Gas separation by mixed matrix membranes with porous organic polymer inclusions within o-hydroxypolyamides containing m-terphenyl moieties, Polymers 13 (2021) 931, https://doi.org/10.3390/polym13060931.
[23] C. Soto, C. Aguilar Lugo, S. Rodríguez, L. Palacio, Á.E. Lozano, P. Prádanos, A. Hernandez, Enhancement of CO2/CH4 permselectivity via thermal rearrangement of mixed matrix membranes made from an o-hydroxy polyamide with an optimal load of a porous polymer network, Separ. Purif. Technol. 247 (2020), 116895, https://doi.org/10.1016/j.seppur.2020.116895.
[24] S. Rico-Martínez, C. Álvarez, A. Hernández, J.A. Miguel, Á.E. Lozano, Mixed matrix membranes loaded with a porous organic polymer having bipyridine moieties, Membranes 12 (2022) 547, https://doi.org/10.3390/membranes12060547.
[25] T. Chen, X. Wei, Z. Chen, D. Morin, S.V. Alvarez, Y. Yoon, Y. Huang, Designing energy-efficient separation membranes: knowledge from nature for a sustainable future, Adv. Membr. 2 (2022), 100031, https://doi.org/10.1016/j.advmem.2022.100031.
[26] G. Ji, M. Zhao, Membrane separation Technology in carbon capture, in: Y. Yun (Ed.), Recent Adv. Carbon Capture Storage, IntechOpen, Rijeka, 2017, https://doi.org/10.5772/65723.
[27] S.C. Rodrigues, M. Andrade, J. Moffat, F.D. Magalhães, A. Mendes, Carbon membranes with extremely high separation factors and stability, Energy Technol. 7 (2019), 1801089, https://doi.org/10.1002/ente.201801089.
[28] G. Clarizia, Strong and weak points of membrane systems applied to gas separation, Chem. Eng. Trans. 17 (2009) 1675–1680, https://doi.org/10.3303/CET0917280.
[29] J.-F. Zhao, L. Chen, P.-J. Sun, X.-Y. Hou, X.-H. Zhao, W.-J. Li, L.-H. Xie, Y. Qian, N.-E. Shi, W.-Y. Lai, Q.-L. Fan, W. Huang, One-pot synthesis of 2-bromo-4,5-diaza-fluoren-9-one via a tandem oxidation–bromination-rearrangement of phenanthroline and its hammer-shaped donor–acceptor organic semiconductors, Tetrahedron 67 (2011) 1977–1982, https://doi.org/10.1016/j.tet.2010.12.065.
[30] A.R. Cruz, M.C.G. Hernandez, M.T. Guzmán-Gutiérrez, M.G. Zolotukhin, S. Fomine, S.L. Morales, H. Kricheldorf, E.S. Wilks, J. Cárdenas, M. Salmón, Precision synthesis of narrow polydispersity, ultrahigh molecular weight linear aromatic polymers by A 2 + B 2 nonstoichiometric step-selective polymerization, Macromolecules 45 (2012) 6774–6780, https://doi.org/10.1021/ma301691f.
[31] M.T. Guzmán-Gutiérrez, D.R. Nieto, S. Fomine, S.L. Morales, M.G. Zolotukhin, M.C. G. Hernandez, H. Kricheldorf, E.S. Wilks, M.T. Guzmán-Gutiérrez, D.R. Nieto, S. Fomine, S.L. Morales, M.G. Zolotukhin, M.C.G. Hernandez, H. Kricheldorf, E. S. Wilks, M.T. Guzmán-Gutiérrez, D.R. Nieto, S. Fomine, S.L. Morales, M. G. Zolotukhin, M.C.G. Hernandez, H. Kricheldorf, E.S. Wilks, Dramatic enhancement of superacid-catalyzed polyhydroxyalkylation reactions, Macromolecules 44 (2011) 194–202, https://doi.org/10.1021/ma102267f.
[32] M.T. Guzmán-Gutiérrez, M.G. Zolotukhin, D. Fritsch, F.A. Ruiz-Treviño, G. Cedillo, E. Fregoso-Israel, C. Ortiz-Estrada, J. Chavez, C. Kudla, Synthesis and gas transport properties of new aromatic 3F polymers, J. Membr. Sci. 323 (2008) 379–385, https://doi.org/10.1016/j.memsci.2008.06.041.
[33] S. Sánchez-García, F.A. Ruiz-Treviño, M.J. Aguilar-Vega, M.G. Zolotukhin, Gas permeability and selectivity in thermally modified poly(oxyindole biphenylylene) membranes bearing a *tert* -butyl carbonate group, Ind. Eng. Chem. Res. 55 (2016), https://doi.org/10.1021/acs.iecr.6b01304 acs.iecr.6b01304.
[34] BIOVIA, Materials Studio, 2017R2, San Diego, Dassault Systèmes, 2017. https://3ds.com/products-services/biovia/products#_ga=2.150667057.647335877.1602788749-a1fe2030-0f18-11eb-9e30-4f2b8d558f14.
[35] HyperChem(TM), Professional (Version 8.0.3), Hypercube, Inc., Florida, USA, 2011.
[36] M.J.S. Dewar, E.G. Zoebisch, E.F. Healy, J.J.P. Stewart, Development and use of quantum mechanical molecular models. 76. AM1: a new general purpose quantum mechanical molecular model, J. Am. Chem. Soc. 107 (1985) 3902–3909, https://doi.org/10.1021/ja00299a024.
[37] I.Y. Zhang, J. Wu, X. Xu, Extending the reliability and applicability of B3LYP, Chem. Commun. 46 (2010) 3057–3070, https://doi.org/10.1039/c000677g.

[38] J.B. Foresman, A. Frisch, Exploring Chemistry with Electronic Structure Methods, 1996.
[39] I. Frisch, (Gaussian, Inc.), Michael J. Trucks (Gaussian, Inc.), G. W. Schlegel (Gaussian, Inc.), H. Bernhard (Gaussian, Gaussian 09, Revision A.02, Gaussian 09, Revis. A.02, 2009.
[40] R. Dennington, T. Keith, J. Millam, GaussView, Version 5, Semichem Inc., Shawnee Mission. KS, 2009.
[41] D.R. Nieto, S. Fomine, M.G. Zolotukhin, L. Fomina, M. Del Carmen Gutiérrez Hernandez, M. del C.G Hernandez, Superelectrophilic activation of N -substituted isatins: implications for polymer synthesis, a theoretical study, Macromol. Theory Simul. 18 (2009) 138–144, https://doi.org/10.1002/mats.200800075.
[42] M. Calle, A.E. Lozano, J. de Abajo, J.G. de la Campa, C. Álvarez, Design of gas separation membranes derived of rigid aromatic polyimides. 1. Polymers from diamines containing di-tert-butyl side groups, J. Membr. Sci. 365 (2010) 145–153, https://doi.org/10.1016/j.memsci.2010.08.051.
[43] C. Álvarez, Á.E. Lozano, M. Juan-y-Seva, J.G. de la Campa, Gas separation properties of aromatic polyimides with bulky groups. Comparison of experimental and simulated results, J. Membr. Sci. 602 (2020), 117959, https://doi.org/10.1016/j.memsci.2020.117959.
[44] M. Calle, C.M. Doherty, A.J. Hill, Y.M. Lee, Cross-linked thermally rearranged poly (benzoxazole- co -imide) membranes for gas separation, Macromolecules 46 (2013) 8179–8189, https://doi.org/10.1021/ma4014115.
[45] J.L. Santiago-García, C. Álvarez, F. Sánchez, J.G. de la Campa, Gas transport properties of new aromatic polyimides based on 3,8-diphenylpyrene-1,2,6,7-tetracarboxylic dianhydride, J. Membr. Sci. 476 (2015) 442–448, https://doi.org/10.1016/j.memsci.2014.12.007.
[46] C. Álvarez, A.E. Lozano, J.G. de la Campa, G. José, High-productivity gas separation membranes derived from pyromellitic dianhydride and nonlinear diamines, J. Membr. Sci. 501 (2016) 191–198, https://doi.org/10.1016/j.memsci.2015.11.039.
[47] W.J. Box, M.T. Webb, M. Galizia, Evaluating the experimental uncertainty in gas and vapor sorption/adsorption measurements: fundamental considerations and experimental design implications, Ind. Eng. Chem. Res. 61 (2022) 9856–9868, https://doi.org/10.1021/acs.iecr.2c01414.
[48] L.M. Robeson, Correlation of separation factor versus permeability for polymeric membranes, J. Membr. Sci. 62 (1991) 165–185, https://doi.org/10.1016/0376-7388(91)80060-J.
[49] L.M. Robeson, The upper bound revisited, J. Membr. Sci. 320 (2008) 390–400, https://doi.org/10.1016/j.memsci.2008.04.030.
[50] D.F. Sanders, Z.P. Smith, R. Guo, L.M. Robeson, J.E. Mcgrath, D.R. Paul, B. D. Freeman, Energy-efficient polymeric gas separation membranes for a sustainable future: a review, Polymer 54 (2013) 4729–4761, https://doi.org/10.1016/j.polymer.2013.05.075.